Sedimentary Geology 237 (2011) 73–83

Contents lists available at ScienceDirect

Sedimentary Geology

journal homepage: www.elsevier.com/locate/sedgeo

Fired glaciofluvial sediment in the northwestern Andes: Biotic aspects of the Black Mat

William C. Mahaney [a,*], David Krinsley [b], Kurt Langworthy [b], Volli Kalm [c], Tony Havics [d,e], Kris M. Hart [f], Brian P. Kelleher [f], Stephane Schwartz [g], Pierre Tricart [g], Roelf Beukens [h]

[a] Quaternary Surveys, 26 Thornhill Ave., Thornhill, Ontario, Canada L4J 1J4
[b] Department of Geological Sciences, University of Oregon, Eugene, OR 97403–1272, USA
[c] Institute of Ecology & Earth Sciences, Tartu University, Tartu EE51014, Estonia
[d] pH2 LLC, 5250 E US 36, Suite 830, Avon, IN 46123, USA
[e] McCrone Institute, Chicago, IL, USA
[f] School of Chemical Sciences, Dublin City University, Glasnevin, Dublin 9, Ireland
[g] IS Terre, CNRS, Université of Grenoble I, Grenoble, France
[h] IsoTrace Laboratory, Department of Physics, University of Toronto, Toronto, Ontario, Canada M5S 1A7

ARTICLE INFO

Article history:
Received 31 July 2010
Received in revised form 2 February 2011
Accepted 16 February 2011
Available online 23 February 2011

Editor: M.R. Bennett

Keywords:
Chemistry of the Black Mat
Bacteria associated with fired sediment
Diagenesis of the fired material

ABSTRACT

Fired glaciofluvial beds in outwash considered to date from the onset of the Younger Dryas Event (~12.9 ka) in the northwestern Venezuelan Andes are considered equivalent to the Black Mat deposits described in other areas of North and South America and Europe. It may be equivalent to sediment recovered from other sites containing beds with spikes of cosmic nuclides and charcoal indicating the presence of widespread fire, one of the signatures of the Black Mat conflagration that followed the proposed breakup of *Comet Encke* or an unknown asteroid over the Laurentide Icesheet at 12.9 ka. In the northern Andes at Site MUM7B, sediment considered coeval with the Black Mat contains glassy carbon spherules, tri-coatings of C welded onto quartz and feldspar covered with Fe and Mn. Monazite with excessive concentrations of REEs, platinum metals including Ru and Rh, possible pdf's, and disrupted/brecciated and microfractured quartz and feldspar from impacting ejecta and excessive heating summarize the data obtained so far. The purpose of this paper is to document the physical character, mineralogy and biotic composition of the Black Mat.

1. Introduction

Interruption of the Bølling/Allerød warming event (Liu et al., 2009) and sudden onset of the YD cooling event (~12.9 ka) has been the subject of interest of many researchers (Birkeland et al., 1989; Reasoner et al., 1994; Hansen, 1995; Osborn et al., 1995; Van der Hammen and Hooghiemstra, 1995; Rodbell and Seltzer, 2000; Shannahan and Zreda, 2000; Teller et al., 2002; Mahaney et al., 2007a, 2008) over the years. Recent synchronization of paleoenvironmental events in the North Atlantic (Lowe et al., 2008) show an abrupt warm perturbation of climate ca. 14.7 ka, followed by slow but sustained cooling as deduced from ^{18}O concentrations culminating in a sustained cold event (GS 1), beginning 12.9 ka and lasting for just over 1 kyr. Because the YD Event coincided with the Clovis extinction it has wide implications regarding ecological disruption over large areas of North America and Europe, and with this paper, South America as well. A number of hypotheses have been invoked to explain the YD and Clovis–Megafaunal-age extinctions including an impact event (Firestone et al., 2007a,b; Haynes, 2008; Kennett et al., 2007, 2008, 2009), the most recent (Napier, 2010) focusing on the breakup of *Comet Encke* over the Laurentide Icesheet at 12.9 ka. Black Mat sediment in North America and Europe characteristically contain materials representative of glassy carbon spherules, magnetic spherules, platinum metals usually with Ir, pdf's (planar deformation features) in fine grained material, fragmental quartz and feldspar, monazite with high concentrations of light and heavy REEs., along with occasional nanodiamond (lonsdaleite). Despite contrary hypotheses regarding the origin of the YD (Quade et al., 1998; Pinter and Ishman, 2008), the growing number of sites containing Black Mat beds deserves concerted study as to the composition of the material, property characteristics and variance over wide interhemispheric areas, and relation to a cosmogenic origin.

The perturbation that reversed climatic warming led to the rapid advance of YD ice, almost instantaneous in geologic time, is one that deserves concerted study by stratigraphers to determine the composition of the material to support or refute a cosmic origin. More importantly, researchers should re-evaluate and re-study important

* Corresponding author.
E-mail addresses: arkose@rogers.com (W.C. Mahaney), krinsley@uoregon.edu (D. Krinsley), klangwor@uoregon.edu (K. Langworthy), volli.kalm@ut.ee (V. Kalm), aahavics@pH2LLC.com (T. Havics), hart.kris1@gmail.com (K.M. Hart), brian.kelleher@dcu.ie (B.P. Kelleher), schwart@ujf-grenoble.fr (S. Schwartz), pierre.tricart@ujf-grenoble.fr (P. Tricart), roelf.beukens@utoronto.ca (R. Beukens).

0037-0738/$ – see front matter © 2011 Elsevier B.V. All rights reserved.
doi:10.1016/j.sedgeo.2011.02.005

sections to determine if the Black Mat beds have been overlooked. It may be difficult to identify the Black Mat if the ejecta impacted soils but bog, glaciolacustrine and fluvial sediments should contain thin beds of incoming ash and resultant wildfires generating soot (Stich et al., 2008) similar to what is discovered and described herein.

The proposed impact/airburst would have generated a shock wave introducing high velocity ejecta into the atmosphere, most likely penetrating to depth into the stratosphere, an event felt between hemispheres, and possibly deep into South America. If, as proposed (Napier, 2010), the airburst/impact is related to *Comet Encke*, the estimated 200-km wide cometary mass might be expected to have spread ejecta in a wide arc, the most recent evidence coming from the Carolinas (East Coast U.S.) where pdf's and lonsdaleite have been identified (http://scienceforums.com/topic/12199-the-carolina-bays/). Possible Black Mat sediments have been identified in Lake Potrok, coastal Argentina, the evidence based on $^{10}Be/^{9}Be$, reduced O and charcoal at approximately 12.9 ka in recovered sediment (Kim, 2010).

The Black Mat samples described herein (Fig. 1A, B for location; Fig. 2A for stratigraphy) were first thought to have been produced by a lightning strike, similar to events previously described by Barnett (1911) and Blackwelder (1927), and thus this is the interpretation Mahaney et al. (2008) provided in a stratigraphic assessment of YD sites in the northern Andes. After assessment of the encrusted material in the "burnt layer" which showed the welded character of carbon, presence of platinum metals, and glassy C-spherules, amongst other indices hinting of a cosmic event, expanded SEM/EDS analysis of the remaining sample showed the grains were severely brecciated and disaggregated partly by extreme heating and particle impact. Turning then to experimentally heated quartz and feldspathic minerals (Mahaney et al., 2010b) it proved possible to show the temperatures involved were much higher than what a normal terrestrial lightning-produced conflagration might be expected to produce. Since the environment at the time the carbon mat was produced was incapable of producing a carbon mat half a micron in thickness the ingress of carbon from an airburst produced by a meteorite or comet became something more than a mere possibility.

The analysis described herein is intended to document the carbon/biotic composition of the Black Mat identified in the northwestern Andes and to review the criteria thus far identified to substantiate a cosmic event.

2. Regional geology

The criteria for the YD impact is similar to that used to prove the K/T impact (Hildebrand, 1993) with the exception that the Andean evidence is in metamorphic terrane which was heavily glaciated at the time of impact. The section investigated is located at 3800 m a.s.l. (Fig. 1A) and contains deposits of glaciolacustrine and fluvial sediments, the Black Mat situated at the base of an outwash fan of YD age. The Black Mat beds overlie alluvial clayey beds with peat, the latter dated to 11.4 and 11.8 ^{14}C years BP, converted to calibrated calendar years of 13.8–13.4 and; 14.1–13.3 ka cal BP at 235 cm depth and 13.5–13.1 ka cal BP at 232 cm depth. The Black Mat, resident in beds 20 cm above the dated beds lies within the YD window, the glaciofluvial materials escaping the advance of YD ice from above in the catchment.

The Mucuñuque Catchment (Fig. 1A and B), a near linear fault-controlled glacial basin with headwaters on the western slopes of Pico Mucuñuque (4672 m a.s.l.), is the type locality in which the Black Mat (Fig. 1B) was discovered. Pico Mucuñuque is the major high summit north of the Humboldt Massif, the lower valley of which trends SE–NW and is marked by numerous bedrock bars, each punctuated by 100 m drops in elevation down to the elevation of Lago Mucubaji (3600 m a.s.l.). Above 4200 m the valley is floored with bedrock, talus cones dominating the valley sides, and despite earlier claims (Stansell et al., 2005) of Neoglacial moraines, the upper valley lies below the

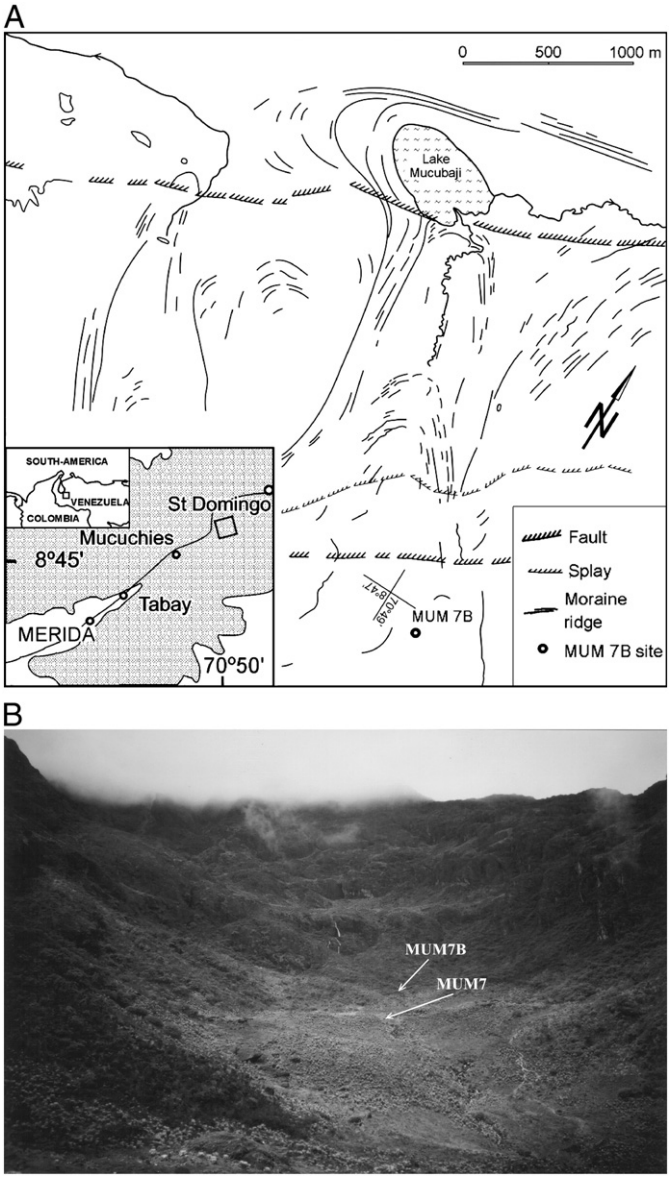

Fig. 1. A. Location of the Black Mat site (MUM7B) in the northwestern Andes. B. Setting of sites MUM7 (Late Glacial moraine succession—YD the upper unit) and MUM7B (outwash overlying glaciolacustrine and glaciofluvial beds including the 2–3 cm thick Black Mat bed.

projected Neoglacial snowline (Mahaney et al., 2007a). Below ca. 4200 m elevation bogs dominate (Salgado-Labouriau and Schubert, 1976) and it is from these source materials and associated thin Mollisols [(NSSC, 1995; Birkeland, 1999) (alpine grassland soils; Mahaney and Kalm, 1996)] that some of the carbon in the Black Mat might have accumulated (see Mahaney et al., 2008). Waterfalls are present wherever bedrock bars are present, a prominent one located just above the MUM7B site where the Black Mat sediment was discovered. During the YD advance this bedrock bar would have been a prominent icefall in the advancing glacier.

Situated between 8°30′ and 9°00′ N and 70°30′ and 70°45′ W, the high summits of the eastern cordillera of the Mérida Andes rise further south, reaching close to 5000 m a.s.l. During the last glaciation [Mérida, Wisconsinan; (Schubert, 1970, 1972, 1974; Mahaney et al., 2007a)], ice spilled northwest from Pico Mucuñuque (Sierra Nevada de Santo Domingo—Fig. 1A) and left a wealth of glacial geomorphic and sedimentological evidence including the Younger Dryas (YD) climatic reversal, the latest event in the Late Glacial record (Ralska-Jasiewiczowa et al., 2001; Gibbard, 2004). This latest of Late Glacial

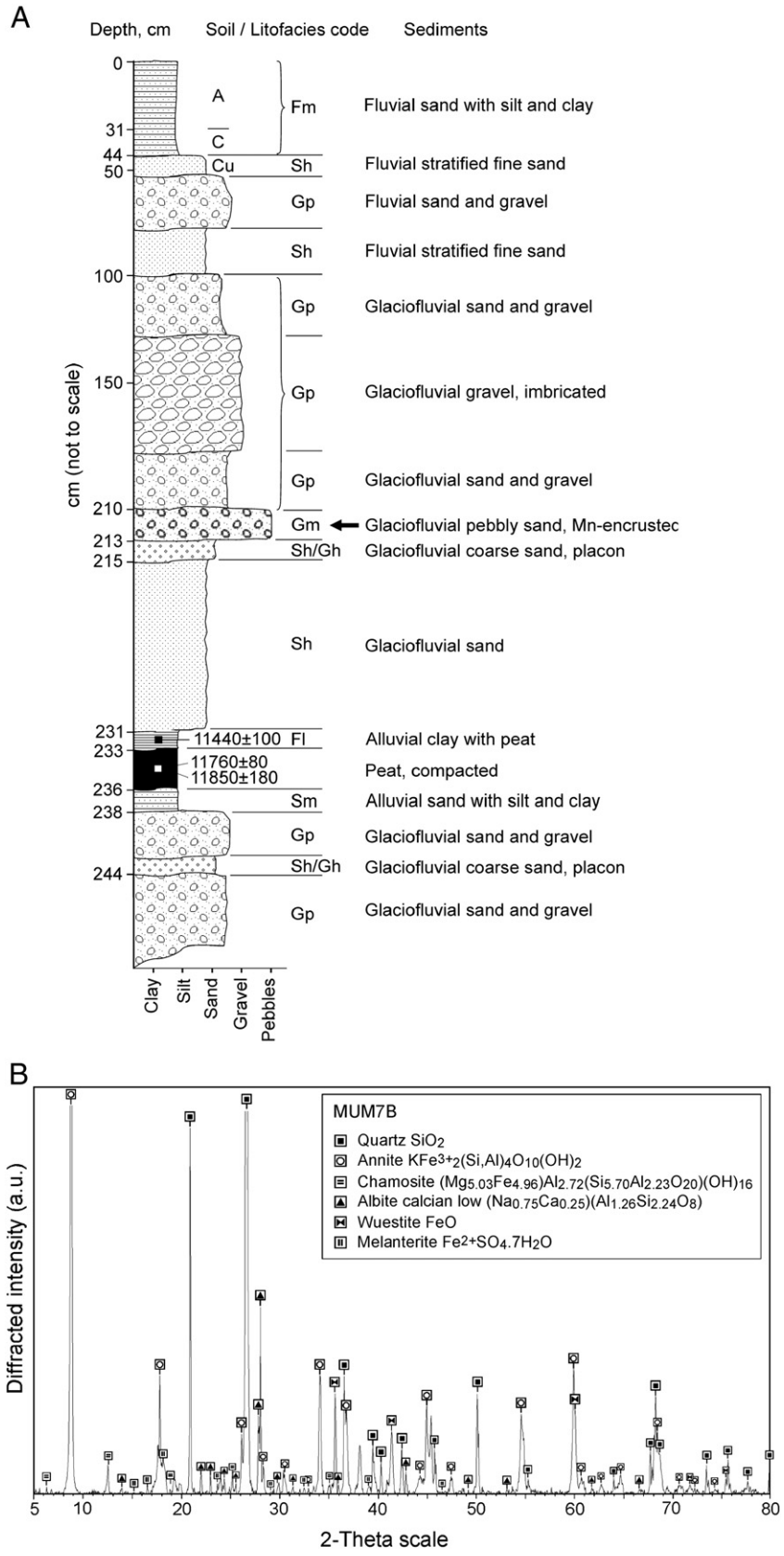

Fig. 2. A. Stratigraphic setting of the Black Mat (arrow for bed location in section), 20 cm above alluvial peat dated to within the Black Mat window of 12.9 ka. B. XRD of the Black Mat bed.

events – the YD – is superimposed on a cooling trend which started 14.7 ka (Lowe et al., 2008), maximum cooling starting at 12.9 ka. The latest review of the YD event by Broecker et al. (2010) puts the YD event into context against the Late Glacial cooling trend, these authors unconvinced of a cosmic spike generating the accelerating cooling necessary to cause a glacial advance that lasted for 1 kyr.

All glacial/fluvial outlets in the research area drained across steep gradients (10–35° slopes) into lacustrine basins located between 3000 and 3600 m a.s.l. Within the Mucubají Valley upstream of the previously documented recessional moraine sites (Mahaney and Kalm, 1996; Mahaney et al., 2008) new investigations reveal geomorphologic and stratigraphic information (including surface moraine and outwash fans burying alluvial peat), all of which document a resurgence of ice following the breakup and retreat of glaciers in the Late Glacial, the youngest suite of sediments corresponding to the YD. Ice overran older Late Glacial deposits consisting of tills, glaciolacustrine and/or glaciofluvial deposits, leaving buried organic materials which date to between 13.7 and 12.4 ka cal BP, together with reworked peat dating to 18.8 ka cal BP.

3. Materials and methods

The Black Mat bed, a 2–3 cm thick encrustation of C + Fe + Mn on pebbly sand of felsic gneiss and granitic composition, is found near the base of the MUM7B (Fig. 2A) section at 3800 m a.s.l. in Mucuñuque Valley. As shown in Fig. 2A the burnt layer material was first thought to result from a lightning strike and resultant fire, although the conflagration temperature in a wet tundra undergoing first or second stage succession vegetation growth would not be high, certainly not high enough to produce glassy C-rich spherules firmly fixed to mineral surfaces. Admittedly, the C-spherules could be attributed to low redox potential, however, the association with carbon welded onto quartz, dislocated quartz, pdf's, brecciated quartz surfaces presumably resulting from impact led to a testable hypothesis more in line with previously reported data (Mahaney et al., 2010a,b). The burnt layer material was later renamed (Mahaney et al., 2010a) and correlated with the Black Mat beds described elsewhere in North and South America and Europe.

The section was dug by hand and cut back to expose a fresh face. The entire section was collected for laboratory analysis and peats and organic clayey alluvial silts were collected for radiocarbon dating as explained by Mahaney et al. (2008, 2010a). Samples for ^{14}C dating were handled with metal implements, air-dried, and wrapped in aluminum foil and prepared for laboratory processing, the radiocarbon samples analyzed within one month of collection. At the IsoTrace Radiocarbon Laboratory in the University of Toronto, all samples were chemically pretreated before AMS dating. Samples were first treated with hot 4 N HCl, followed by extraction with freshly prepared 0.25 N NaOH and acid washed to remove possible carbonate and humic contaminants. As part of the pretreatment, the clayey silt sample (TO-9278a) was first demineralized in hot HCl and HF. The resultant dates are corrected for isotopic fractionation and are calibrated with the OxCal v.3.10 calibration program (Bronk-Ramsey, 2005) using the INTCAL04 calibration data for the Northern Hemisphere (Reimer et al., 2004). In a previous publication (Mahaney et al., 2008) the uncertainties of the ^{14}C dates are reported as 1σ, whereas calibrated ^{14}C ages are reported as 2σ ranges. The calibrated results, quoted in this paper, are the medians of these 2σ ranges.

Sediment/soil samples from the MUM7B site were air-dried and subjected to particle size analysis following procedures outlined by Day (1965). Sands separated by particle size analysis and samples recovered from encrustations on pebbles in an upper placon at MUM7B were dried and subsampled under the light microscope. Selected grains were then mounted on stubs for analysis by Field Emission Scanning Electron Microscope (FESEM), normal SEM (SE) and Energy-Dispersive Spectrometry (EDS) following methods outlined by Mahaney (2002). When analyzing for carbon, samples were coated with gold–paladium or thinly carbon coated, the C tested against a carbon coated stub to estimate the spectral concentration; when analyzing silicates samples were coated with C (Vortisch et al., 1987; Mahaney, 2002). Photomicrographs were obtained at accelerating voltages of 10 to 20 keV. X-ray microanalysis was acquired at an accelerating voltage of 10 keV.

Some samples were analyzed with a TEM (Transmission Electron Microscope) and FIB (Focused Ion Beam). Fragments of rock from the Black Mat were attached to an aluminum SEM stub with epoxy and allowed to dry. The fragments were examined and photographed with a reflected light microscope in order to locate initial areas of interest. After light microscopy, the sample was imaged in secondary electron (SE) mode, using an FEI Helios dual-beam focused ion beam (DB-FIB) microscope. A thin layer of Pt metal was deposited *in situ* with the DB-FIB to help protect the outermost surface from ion beam damage, and to decrease curtaining defects often observed while milling dissimilar materials (Formanek and Bugiel, 2006). After Pt deposition, ion beam milling at 30 kV, 2.8 nA was performed on each side of the region of interest to create a one-micron wide region for cross-section lift out. The region of interest was cut free from the bulk material using the ion beam, then lifted out with the use of an Omniprobe micromanipulator and attached to a copper TEM grid using a platinum gas precursor. We ion thinned and polished our specimens at low beam currents; this allowed us to carefully monitor the thickness of our specimens, as well as to minimize accidental beam damage to the specimens. The cross-section was further thinned and ion polished at 5 kV, 16 pA using the DB-FIB to produce an approximately 100 nm thick specimen for HR-TEM analysis. HR-TEM analysis was performed with an image-

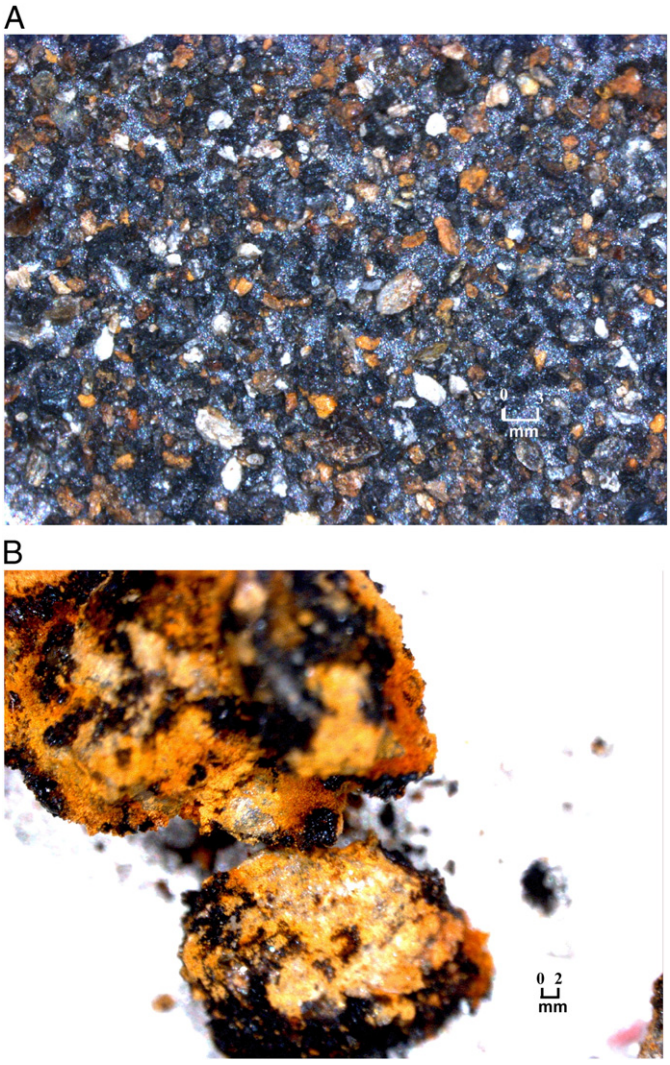

Fig. 3. A. Black Mat grains under the light microscope. B. Enlargement of Black Mat grains. Dark areas indicate Fe–Mn encrustation with C glass spherules.

corrected, FEI Titan transmission electron microscope. Images of the Black Mat sample were obtained with a high angle annular dark-field (HAADF) STEM detector. Chemical analysis was performed while imaging in STEM mode with an EDAX EDS detector.

A portion of the Black Mat sample was sieved into fractions (1 mm, 500 μm, 250 μm, 180 μm, 90 μm, and <90 μm). The 90 μm fraction was mounted under an Olympus BH2 fluorescent microscope. The fluorescent microscope was used at 100×–450× to evaluate primary fluorescence, then secondary fluorescence after application of Acridine Orange (AO). AO has been utilized for the detection of bacteria and in this case the residual indications of bacteria (Bowden, 1977; Hobbie et al., 1977; Clark, 1981; Palmgren et al., 1986).

XRD patterns were recorded with a Bruker D5000 powder diffractometer equipped with a SolX Si(Li) solid state detector from Baltic Scientific Instruments using CuKa_1 + 2 radiation. Intensities were recorded at 0.04° 2-theta step intervals from 2 to 50°, using a 45 s counting time per step. Sizes of the divergence slit, the two Soller slits, the antiscatter, and resolution slits were 0.5°, 2.3°, 0.5° and 0.06°, respectively.

Black encrusted samples were subjected to Laser Raman analysis at the Ecole Normale Supérieure (ENS)-Lyon. A LABRAM HR800 double subtractive spectrograph with premonochromator and nitrogen-cooled SPECTRUM1 CCD detector was used in the analysis. The premonochromator, equipped with confocal optics before the spectrometer entrance, achieved excitation using a laser beam with a wavelength of 514.5 nm. The laser beam was focused using a microscope equipped with a ×50 objective and the Raman signal was collected in the backscatter direction. A confocal pinhole before the spectrometer allows a sampling

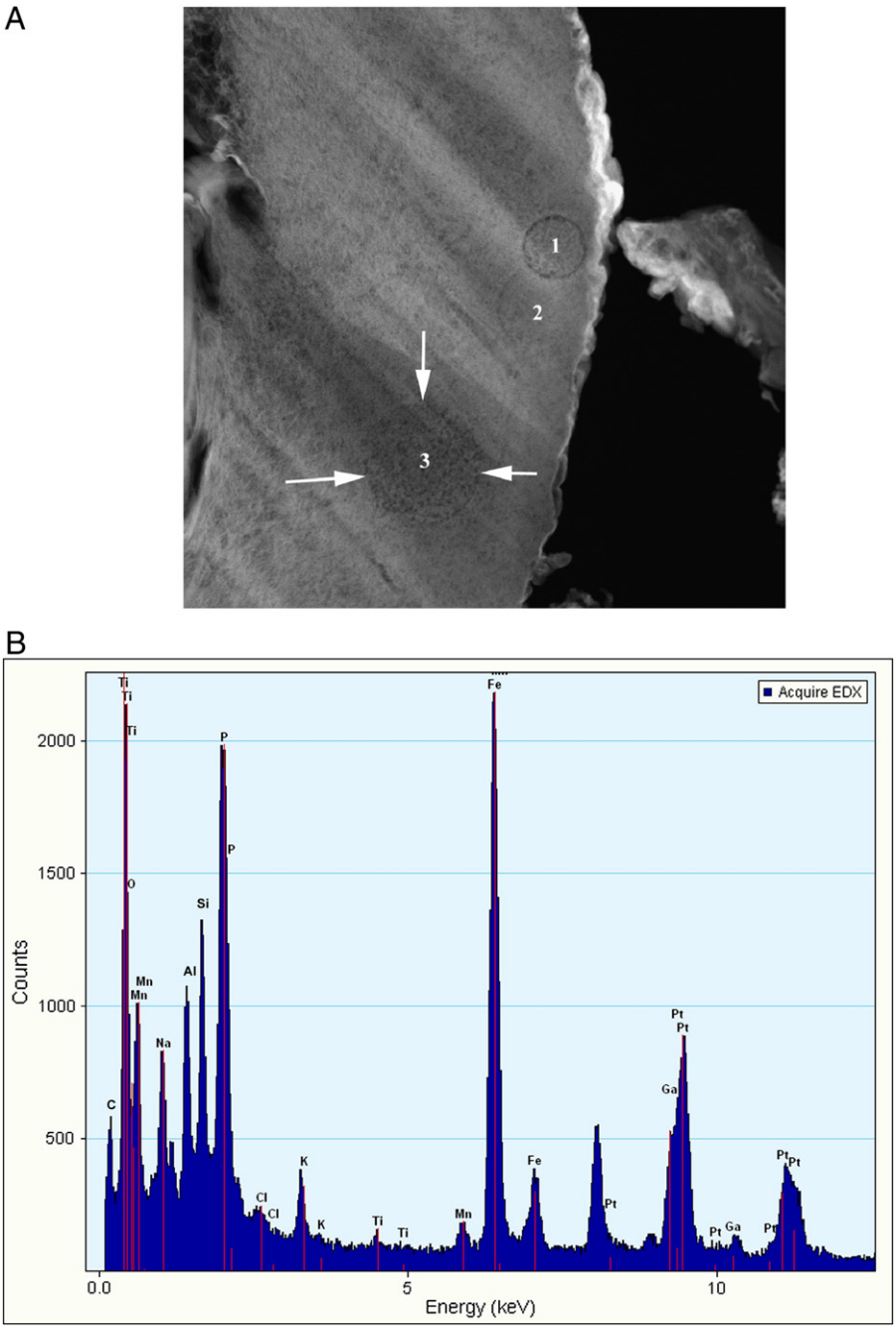

Fig. 4. A. General area of numbered bacteria cells in the Black Mat surface. Image taken with the TEM. Tonal contrast is considered to reflect elemental composition—dark areas on nodes are high in C, light areas high in Fe–Mn; B. EDS of panel A showing C mat on K-spar/rutile intergrowth with high P, possibly monazite but without REEs.

of about 2 to 5 μm-size analytical zone. The laser power was 400 mW at the sample surface. Acquisition time-span was about 180 s distributed during three accumulating cycles.

4. Results

The mixed mineral/encrusted matter composition determined by XRD (Fig. 2B) shows the primary mineral component to consist largely of quartz, albite, annite, chamosite, melanterite and wuestite, the latter a Fe^{+2} oxide found in native Fe deposits and in meteorites. Significant chlorite and illitic clay minerals are also present along with Mn oxides of variable composition, the latter probably weathering products related to fluctuating redox conditions. No stishovite or diamond was identified in the analysis.

The general field of view (Fig. 3A), taken with the light microscope, shows minerals in the Black Mat bed, some more heavily encrusted with carbon than others, all exhibiting colors of black (10YR–5YR 1.7/1) and reddish black (2.5YR 1.7/1; Oyama and Takehara, 1970). An enlarged view with the light microscope (Fig. 3B) gives a better impression of the globules of C-encrusted material spread randomly across microlaminated sediment. The encrusted C occurs both *in situ* by itself, sometimes fixed on a Fe–Mn substrate and most often welded onto mineral surfaces overlain with Fe and Mn, the latter considered to result from fluctuating redox conditions. The bed is associated with placons down section, which have acted as aquifers but lack C-encrusted material.

Imaging of randomly spaced microbial cells on the carbon-encrusted Black Mat surface is shown in Figs. 4A and 5A, with some cells exhibiting extreme diagenesis but with either an entire or partial cell wall intact. The microbes are considered to be pseudomorphs of once living colonies that may have proliferated over a much greater carbon–Mn-encrusted surface, the C remaining as residue, while, as shown in Figs. 4B and 5B, the N was presumably completely taken up in the gas cycle. Manganese oxidation by bacteria (Nealson, 1983; Bougerd and De Vrind, 1987) probably explains much of the Mn found as coating on grains in the Black Mat bed, the remainder coming from redox fluctuations in the aquifers (placons; Tilsley, 1977) resident in the section, or possibly from the impact itself (Schüssler et al., 2002). Crenulated or scalloped quartz shown in Fig. 6A is partly free of C coating but contains some Al and Cl. The Al could be scavenged from other country rock minerals especially sillimanite or andalusite but the Cl, while unexplained, could be related to aluminosilicate glasses and have an interstellar origin (Stebbins and Du, 2002). Disrupted quartz on a scale such as shown here can only be explained by some combination of impact and heat as discussed by Mahaney et al. (2010b).

The clear spheroid shaped object resembling a coccoid cell is shown (No. 1) in Fig. 4A. The size is estimated to be approximately 300 nm making it of suitable size for bacteria or Archaea (Huber et al., 2002). At this size they are still extremely small but not enough to indicate they are abiotic in origin (Maniloff et al., 1997).

The darker surrounding area showing the circular nature of the object clearly resembles a cell wall and could be the result of mineralization of extracellular polysaccharide substances (EPS) or

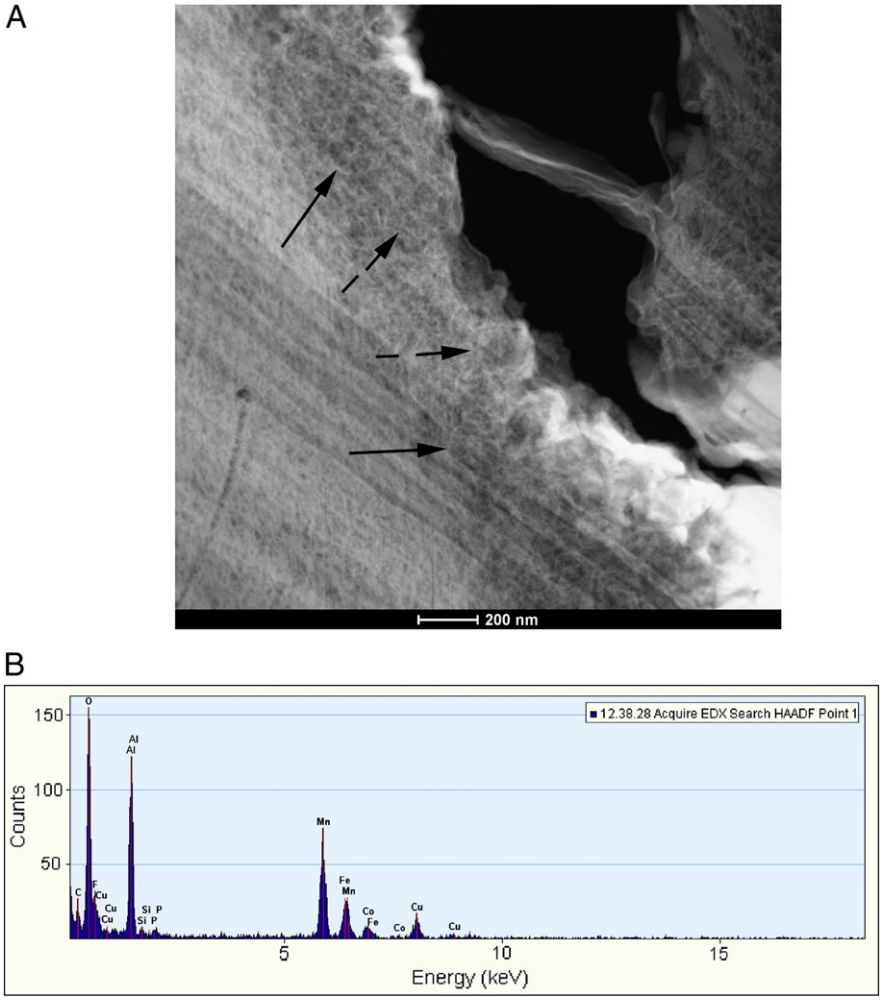

Fig. 5. A. High resolution STEM image of bacteria on the Black Mat surface. Solid arrows indicate bacterium with little diagenesis. Dashed arrows depict bacterium somewhat degraded. Integrated bacteria formed into colonies adjacent to the fired surface. B. EDS of bacteria.

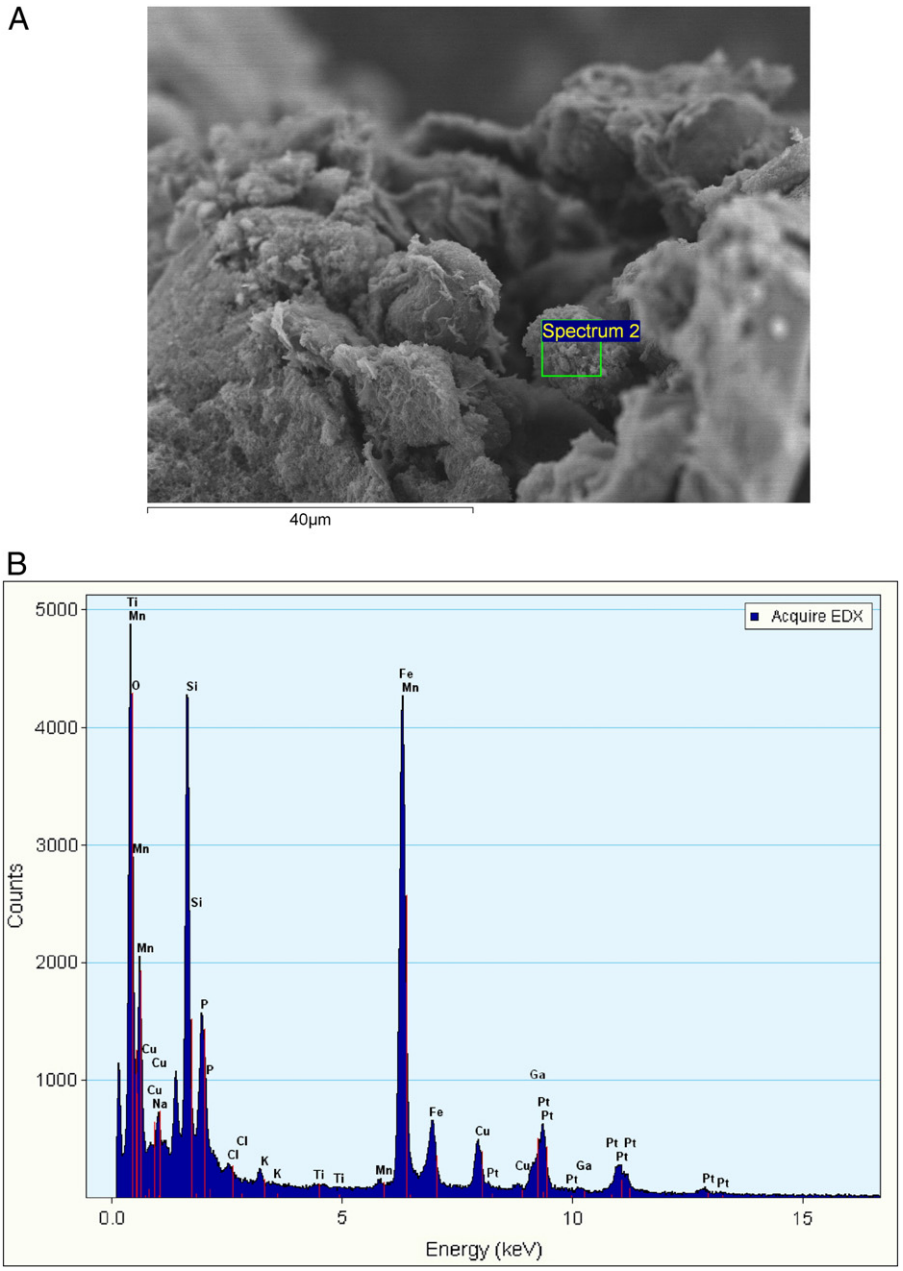

Fig. 6. A. Fine silt size grains encrusted with Black Mat coating. B. EDS spectrum showing Fe/Mn and C encrusted on quartz.

both (Westall et al., 2001). It is also evident that the inner region of this sphere is darker than the surrounding material possibly due to different mineral interaction during diagenesis of the cytoplasm. Lacking an observable nucleus the cell is probably prokaryotic or an endospore. A faint outline of a sister cell (No. 2, Fig. 4A) may be present although it appears to have undergone more diagenesis and exhibits a "ghost like" form. It could be hypothesized that this is a daughter cell lying beneath or on top of the cell above. Another possible cocci microbial fossil of larger diameter (No. 3, Fig. 4A) could be a different species, or a phage infected cell or possibly a eukaryotic cell artifact. The dark spots throughout the formation could be fossilized internal cell components. While this is unlikely some internal cell components such as the cytoplasm may act as nucleation sites for mineralization (Westall et al., 2001). This latter postulate, while possible, is unlikely since there is no observable nucleus.

These cells are representative of the putative bacteria seen in several other images. From the internal structure exhibited in Fig. 5, taken with a STEM, the bacterial cocci annotated (1) of Fig. 4A is shown with the full proliferation of many colonies of bacteria. The intact colonies seem to have undergone only minor diagenesis, which appears to have acted differentially on the material (as indicated by arrows), hydrolyzing only parts of some colonies. The chemistry (Fig. 5B) of the bacterial infestation/colonies shows a different spectrum to that in Fig. 4B with no N, lower C limited presumably to the firing produced by incoming ejecta, which in this instance is welded onto an Al-rich material with plentiful O and little Si, possibly Al glass. Aside from other ions, P suggests the presence of organic material or possibly monazite, although no Th and only minor Ce was detected. The presence of Al in appreciable concentration with trace quantities of Si indicates large quantities of Al (glass). The Pt and Ga are conductive material used to image the sample after extraction with the FIB.

Still other bacterial pseudomorphs were located with the SEM in backscattered mode as shown in Fig. 6A, many of which are located on C-rich globules of material lightly cemented together. However the C-rich surface is either welded to mineral substrates or exists as a

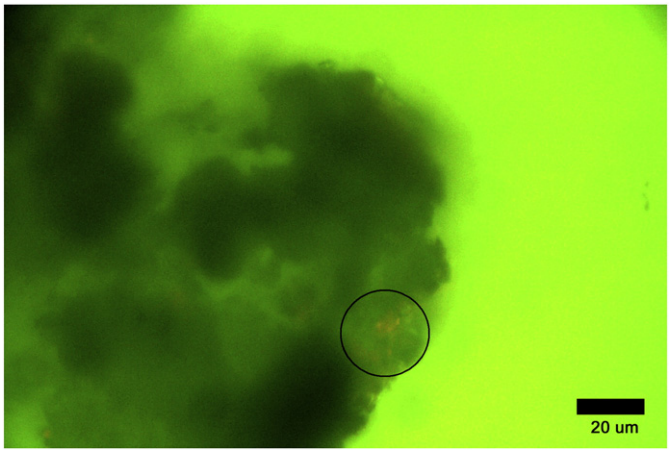

Fig. 7. High resolution microscopic fluorescent image using Acridine Orange to identify bacteria as indicated (circle).

fibrous mat of material. The chemistry of the bacterial artifact in Fig. 6A is shown in Fig. 6B. As before, in Fig. 5B, Pt and Ga are the conductive media. Carbon (unlabeled) may reflect the thickness of Fe and Mn on the sample, the Ti considered to be an intergrowth of rutile and quartz or rutilated quartz. The presence of minor Al and Cl may be related to the original cometary/asteroid material as discussed below. This additional imagery (Fig. 6A) from the Black Mat shows micro concentrations of microfragmental Al, lightly coated with Mn and C (similar to what is in Fig. 3A and B) and surrounded by twisted quartz, similar to what is shown here. Some fragmental material, encased in nodules of ~10 μm diameter, also consists of micro sawtooth forms as seen in Fig. 6A of Mahaney et al. (2010b). The high concentration of Fe indicates the presence of variable Fe oxides including wuestite, biotite, annite and chlorite as indicated in the XRD analysis and maghemite and hematite.

Analysis by Fluorescent Light Microscope (indicates spherical to rod shaped fluorescent response in the 90 μm fraction of the subsample (Fig. 7). The fluorescence was noted on and in the porous structure of the subsample. Sample material from larger sieve fractions did not allow sufficient examination due to limited depth of field in the fluorescent microscope. The fluorescent particles in the <90 μm fraction could not be definitely associated with the proper layer and thus were not relied upon.

Analysis of the Black Mat sediment by Raman spectrometry (Fig. 8) shows several spectral signals with main peaks at 1529 and 1137 cm^{-1} and a large peak at 1360 cm^{-1}, the latter representing the D1 band of carbonaceous matter and the 1597 cm^{-1} band as the G band. Quartz is represented by the 1100 cm^{-1} spectral band. The Raman spectra also depict a broad peak between 1300 and 1600 cm^{-1}, the two interpreted to be a mixture of iron oxides (maghemite and hematite; de Faria et al., 1997) and carbonaceous material. The deconvoluted signal shows a thin band near 1597 cm^{-1} that matches the G band characteristic of distorted graphite (Bény-Bassez and Rouzaud, 1985; Nakamura et al., 1995) and a large band at 1360 cm^{-1} that matches the D1 band corresponding to in plane–plane defects and heteroatoms (Bény-Bassez and Rouzaud, 1985).

5. Discussion

The Black Mat bed shown in Fig. 2A, situated ca. 16 cm above the dated YD beds, falls directly within the YD time window. This poses the question as to the length of time required for deposition of sand between the YD beds and the carbonized encrusted material. The 5-cm thick peat bed shown in Fig. 2A was deposited over 400 years taking the raw dates as standard. At 1 sigma the outside range of time is another 280 years; at two sigma it is 560 years. If the overlying

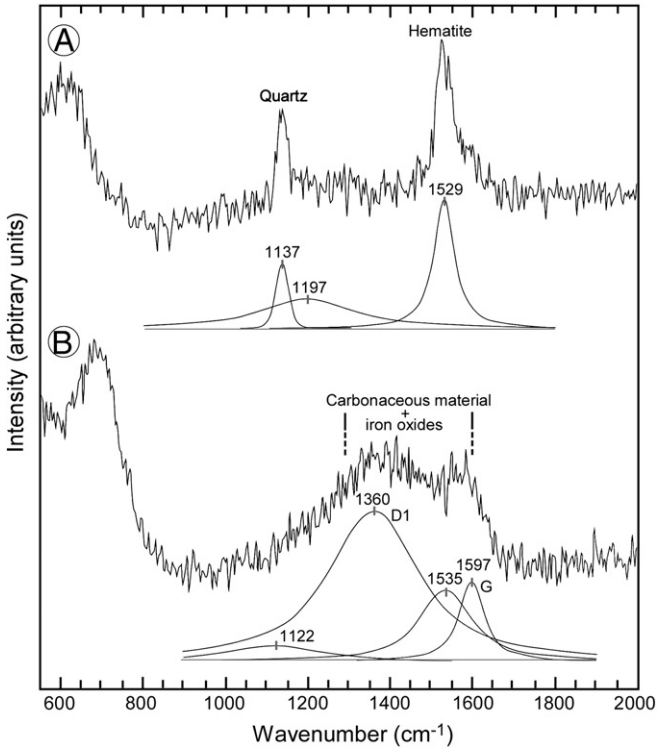

Fig. 8. Typical Raman spectrum obtained from the Black Mat sample. A. The 1100 cm^{-1} spectral band corresponds to quartz and the 1530 cm^{-1} corresponds to hematite. B. Raman spectra shows locally a broad peak between 1300 and 1600 cm^{-1} which is interpreted as a mixture of iron oxide (hematite) and carbonaceous material.

gravel outwash is assumed to have been emplaced near the end of the YD event (Mahaney et al., 2008, 2010a), and if the carbonized encrusted bed is indeed the Black Mat equivalent, it is assumed the YD ice overran both the dated peat beds and the carbon encrusted beds with only very minor deformation. It is further assumed that either the overrun beds were frozen (highly unlikely) or they were at saturation which would have produced hydrostatic pressure with stress acting in every direction, thus preserving the material. The lack of till in the section makes the evidence circumstantial but it is clear the *lowermost extent* of YD ice in the catchment is at 3800 m a.s.l., a full 200 m lower than on the Humboldt Massif, some 50 km to the south (Mahaney et al., 2009). Lack of deformation in tropical glacial sediments is the norm principally since they are often formed under the warmest of all warm glaciers that are losing mass by melting through much of the year (Mahaney, 1990, 2002).

The equilibrium line altitude discrepancy between the Mucuñuque Catchment (~3900 m) and the Humboldt Massif (~4100 m) can only be explained by differences in storm tracks delivering snow to the two drainages or by differences in the geometry of the two source areas. Mucuñuque Catchment is a narrow valley whereas the Humboldt is a wide massif with what would have been a radiating glacial flow, not a concentrated unidirectional vector.

The representative spread of granules and silty sand making up the encrusted material shown in Fig. 3A and B contain a wealth of coated grains, many carbon coated, others with variable stain of Fe, Mn and C. The angularity of nearly all clasts depicts a definite glacial signature verified under the SEM with typical glacial crushing microfeatures (Mahaney, 2002). The encrusted bed materials are part of the outwash stratigraphy, presumably part of the Late Glacial sequence predating the YD event, but containing grains that went through the Late Glacial system during the Allerød or earlier. The higher magnification light microscope image in Fig. 3B gives a strong impression of the coating frequency, intensity and ratio of carbon to Fe/Mn encrustation. What stands out in this image are the angular quartz

grains and the high frequency of glassy carbon spherules, the latter not seen in normal biotic films of argillic horizons in paleosols, fibrous coated silicates associated with YD overrun peats (Mahaney et al., 2009), and peats buried and deformed in Early Mérida (Wisconsin) glaciolacustrine sediments in nearby catchments (Dirszowsky et al., 2005). As reported above, it is the composition of these glassy carbon spherules and associated minerals comprising extraordinary concentrations of REEs that form the principal body of evidence for a cosmogenic impact event.

Because little is known of the effects of firing events on silicate rocks outside of lightning-induced pyrometamorphism (McLintock, 1932; Grapes, 2006), origin of fulgurites (Wright, 1999), magnetic anomalies on artifact materials (Maki, 2005) and presumed lightning-induced wildfiring of timberline vegetation (Mahaney et al., 2007b), a number of firing tests were conducted at the University of Oregon (Mahaney et al.., 2010b) in which quartz and feldspar minerals were heated from 400 to 900 °C, tested at each stage by SEM to determine degree of disaggregation/brecciation and microfracture development. The impact of heat alone achieves a remarkable degree of structural damage to grains, principally to feldspars with fracture lines tending to parallel crystallographic planes. Add to this the input from incoming ejecta from an airburst, fine material traveling at speeds of ca. 25–30 km/s; the release of kinetic energy alone would be sufficient to produce structurally rearranged minerals such as the twisted and deformed quartz and feldspar as described above.

Spherules produced by combustion (similar to welding fumes) suggest very high temperatures and either fast cooling or minimal gravity, particularly with regard to aerodynamic diameter and particle density. Glassy and Fe-based spheres are common from fly ash produced in incinerators and boilers, *e.g.* pleospheres (Fisher et al., 1978; Kuhlbusch, 1995). Coal tends to produce Si-rich glassy spheres with some S, Fe and also K, a product common in biomass burning from plants (Kuhlbusch, 1995). In general, spherical particle formation is caused by condensation of droplets (Mendez et al., 2000; Shukla et al., 2001). It is known that amorphous silica has water loss at 570 °C (Jakes and Mitchell, 1996), and that ashing at 900 °C does not destroy silica bodies in plant material (Lanning et al., 1958). Furthermore, temperatures of 1350 °C or greater are needed for annealing of amorphous silica (Graetsch et al., 1994) and others have concluded that fly ash sphere formation (similar to that seen here) occurs from molten droplets at >1350 °C (Environmental Protection Agency, 1980). Despite observations that no spherical-like particles were discovered in actual field test burning after examination by SEM (Komarek et al., 1973), current findings discussed here indicate temperatures over 1350 °C are needed to produce the C-rich spherules.

Natural and experimentally derived bacterial fossils result in structures displaying the same size, shape, cellular complexity and colonial characteristics as the original organism(s) (Westall et al., 2001). The fossilization of bacteria was experimentally demonstrated by Westall et al. (1995) where the cell wall, EPS and cytoplasm acted as nucleation sites for mineralization. The experiment showed that this led to the almost complete replacement of the organic cell with an encrusted cast. It was assumed that the organic matter of the inner cell degrades and disappears as the cell is fossilized, although some may remain as demonstrated by the EDS spectra obtained in this study. The fossilization of microbial cells can lead to the production of artifacts within the cell body. For example, a false nucleus may form during fossilization because condensation of the cytoplasm during degradation may produce a condensed clot. If this clot is fossilized then a false nucleus may be observed in the center of the structure leading to an incorrect observation that one is looking at a eukaryotic cell. The lack of nucleus however does not discount the possibility that the observed microstructures are of a eukaryotic origin *e.g.* microspores (Bernard et al., 2007).

As reported above, Fig. 4A displays three spherical structural microfeatures contained within the main material Black Mat body, all of which closely resemble coccoid microbial fossils of undetermined age. The sphere denoted here as *sphere 1* contains an obvious circular boundary of darker material that may have formed during diagenesis of the cell wall components. The near perfect circular shape of the structure is curious as some deformation would be expected for a microbial cell of limited rigidity. The proximity of a neighboring spherical structure (*sphere* 2) that appears to be under or overlays *sphere* 1 looks remarkably like a daughter cell after binary fission, although the remains of *sphere* 2 appear to have undergone considerably more diagenesis. *Sphere* 3 is a circular region covering a larger area than both *spheres* 1 and 2. This localized region of darker material is clearly defined and encompasses its internal structure in a uniform fashion. The supposed cell wall structure surrounding this region is not as dense as observed in *sphere* 1, as is obvious when looking at the undeformed curve of the southwestern part of the structure. No nucleus-like structures were observed in any of the discussed spheres leading to the possibility that they are not eukaryotic although the size and shape does not discount the possibility that they may be algal in origin as well.

The identification of bacteria, partially preserved on geological materials, can be exceedingly difficult, especially when workers rely almost exclusively on morphology. Pseudofossil mimics of inorganic mineral microstructures can be difficult to identify and some have been identified in the past (Schopf et al., 2002). Even nano-size sulfate-reducing bacteria can only be identified by differential concentrations of ^{34}S in filaments and spherules (Kucha et al., 2005). For the reason that the identification of nanobacteria relies almost exclusively on TEM analysis (Xu et al., 2003), we believe the results presented here are representative of both fossil and extant forms of bacteria found on Black Mat sediments at the type locality in the northern Andes of Venezuela. All of the macro and nanobacteria forms we have identified on Black Mat grains are of the spherical type (cocci) without spiral (spirilla) or rod (bacilli) shapes (see Schopf, 1999, for bacterial form types). All appear to be unicellular, often formed together in clumps but without grouping into filaments. Larger independent and much larger filament forms in the Black Mat are thought to be fungi, many found embedded in the Fe-rich encrusted material (Mahaney et al., 2010a).

6. Conclusions

While lacking direct confirmatory evidence, the encrusted carbonized bed in the northwestern Venezuelan Andes contains properties similar to Black Mat sediments described elsewhere. It is correlative with a large scale firing event that welded carbon onto silicate grains leaving a glassy carbon spherule coating that is certainly vitreous, associated with brecciated, fractured fine sand and silt grains, presumably resulting from grain impact and wildfire event of some magnitude. The environment in the Andean area at the time would have been wet and in a first or second stage of successional vegetation development, one hardly conducive to provide sufficient organic residue to form the carbonized coatings seen on the samples investigated. That some of the carbon input into the system could have come directly from the airburst has yet to be conclusively proved but is within the realm of possibility.

Compared with firing events of lesser magnitude, affecting similar silicate-rich rocks in alpine areas with reduced vegetation supplying material for ignition, it is the *welded nature* of the C affixed to mineral grains that makes the encrusted beds in the Andes stand apart as requiring a much higher temperature, one that would exceed experimentally tested firing of quartz and feldspar under controlled conditions. To achieve a temperature in excess of 900 °C and an impact capable of brecciating mineral grains, and adding to this mix of data copious amounts of monazite with high REE concentrations, invokes a cosmogenic origin for at least some of the mineral matter discussed here.

Acknowledgments

This research was carried out with funding from Quaternary Surveys, Toronto. We thank the Departments of Materials Science and Geology, University of Toronto and the Department of Geology, University of Oregon for use of several Scanning Electron Microscopes. The authors also wish to thank Dana Johnson (University of Oregon) for use of his high temperature furnace and the Science Foundation of Ireland and the Irish Environmental Protection Agency (STRIVE program) for funding.

References

Barnett, V.H., 1911. An example of disruption of rock by lightning on one of the Lucite hills in Wyoming. Journal of Geology 16, 568–571.
Bény-Bassez, C., Rouzaud, J.N., 1985. Characterisation of carbonaceous materials by correlated electron and optical microscopy and Raman microscopy. In: Reimer, L. (Ed.), Scanning Electron Microscopy. SEM Inc., Chicago, pp. 119–132.
Bernard, S., Benzerara, K., Beyssac, O., Menguy, N., Guyot, F., Brown Jr., G.E., Goffé, B., 2007. Exceptional preservation of fossil plant spores in high-pressure metamorphic rocks. Earth and Planetary Science Letters 262, 257–272.
Birkeland, P.W., 1999. Soils and Geomorphology. Oxford University Press, Oxford, UK. 430 pp.
Birkeland, P.W., Rodbell, D.T., Miller, D.C., Short, S., 1989. Investigaciones en el Parque Nacional Río Abiseo, San Martin. Boletin de Lima 64, 55–64.
Blackwelder, E., 1927. Fire as an agent in rock weathering. Journal of Geology 35, 134–140.
Bougerd, F.C., De Vrind, J.M.P., 1987. Manganese oxidation by *Leptothrix discophora*. Journal of Bacteriology 169, 489–494.
Bowden, W., 1977. Comparison of two-direct-count techniques for enumerating aquatic bacteria. Applied and Environmental Microbiology 33 (5), 1229–1232.
Broecker, W.S., Denton, G.H., Edwards, R.L., Cheng, H., Alley, R.B., Putnam, A.E., 2010. Putting the Younger Dryas cold event into context. Quaternary Science Reviews 29, 1078–1081.
Bronk-Ramsey, C., 2005. OxCal Program v 3.10. University of Oxford Radiocarbon Unit, Oxford, http://www.rlaha.ox.ac.uk/oxcal/oxcal.htm.
Clark, G., 1981. Staining Procedures, 4th Ed. Williams & Wilkins, Baltimore, MD.
Day, P., 1965. Particle fractionation and particle size analysis. In: Black, C.A. (Ed.), Methods of Soil Analysis. American Society of Agronomy, Madison, WI, pp. 545–567.
de Faria, D.L.A., Venancio Silva, S., de Oliveira, M.T., 1997. Raman microscopy of some iron oxides and oxyhydroxides. Journal of Raman Specroscopy 28, 873–878.
Dirszowsky, R.W., Mahaney, W.C., Kalm, V., Bezada, M., Hodder, K., 2005. Lithostratigraphy of the Mérida (Wisconsinan) Glaciation and Pedregal Interstade, Mérida Andes, northwestern Venezuela. Journal of South American Earth Sciences 19, 526–536.
EPA, 1980. Environmental Effects of Western Coal Combustion Part IV Chemical and Physical Characteristics of Coal Fly Ash, EPA 600-3-80-094.
Firestone, R.B., West, A., Kennett, J.P., Becker, L., Bunch, T.E., Revay, Z.S., Schultz, P.H., Belgya, T., Kennett, D.J., Erlandson, J.M., Dickenson, O.J., Goodyear, A.C., Harris, R.S., Howard, G.A., Kloosterman, J.B., Lechler, P., Mayewski, P.A., Montgomery, J., Poreda, R., Darrah, T., Que Hee, S.S., Smith, A.R., Stich, A., Topping, W., Wittke, J.H., Wolbach, W.S., 2007a. Evidence for an extraterrestrial impact 12,900 years ago that contributed to the megafaunal extinctions and the Younger Dryas cooling. Proc. National Academy of Sciences 104, 16016–16021.
Firestone, R.B., West, A., Revay, Z., Belgya, T., Smith, A., Que Hee, S.S., 2007b. Evidence for a massive extraterrestrial airburst over North America 12.9 ka ago. American Geophysical Union Mtg. 07, PP41A sessions, San Francisco, AGU Annual Mtg, 2007, PP41A-02.
Fisher, Gerald L., et al., 1978. Physical and morphological studies of size-classified coal fly ash. Environmental Science & Technology 12 (4), 447–451.
Formanek, P., Bugiel, E., 2006. Specimen preparation for electron holography of semiconductor devices. Ultramicroscopy 106 (4–5), 365–375.
Gibbard, P.L., 2004. Quaternary…now you see it, now you don't. Quaternary Perspectives 14, 89–91.
Graetsch, H., Gies, H., Topalovi, I., 1994. NMR, XRD and IR study on microcrystalline opals. Physics and Chemistry of Minerals 21 (3), 166–175.
Grapes, Rodney, 2006. Pyrometamorphism. Springer, NY. 276 pp.
Hansen, B.C.S., 1995. A reevaluation of the evidence for a Younger Dryas climatic reversal in the tropical Andes. Quaternary Science Reviews 12, 769–779.
Haynes, C. Vance, 2008. Younger Dryas "black mats" and the Rancholabrean termination in North America. Proc. National Academy of Sciences 105, 6520–6525.
Hildebrand, A.R., 1993. The Cretaceous/Tertiary boundary impact (or the dinosaurs didn't have a chance). Journal Royal Astronomic Society, Canada 87, 77–117.
Hobbie, J.E., Dalley, R.J., Jasper, S., 1977. Use of nuclepore filters for counting bacteria by fluorescence microscopy. Applied and Environmental Microbiology 33 (5), 1225–1228.
Huber, H., Hohn, M.J., Rachel, R., Fuchs, T., Wimmer, V.C., Stetter, K.O., 2002. A new phylum of Archaea represented by a nanosized hyperthermophilic symbiont. Nature 417, 63–67.
Jakes, K., Mitchell, J.C., 1996. Cold plasma ashing preparation of plant phytoliths and their examination with SEM and EDX. Journal of Archaeological Science 23 (1), 149–156.
Kennett, J.P., Becker, L., West, A., 2007. Triggering of the Younger Dryas Cooling by extraterrestrial impact. AGU Annual Mtg, 2007, PP41A-05.
Kennett, D.J., Kennett, J.P., West, G.J., Erlandson, J.M., Johnson, J.R., Hendy, I.L., West, A., Culleton, BmJ, Jones, T.L., Stafford Jr., T.W., 2008. Wildfire and abrupt ecosystem disruption on California's Northern Channel Islands at the Ållerød–Younger Dryas boundary (13.0–12.9 ka). Quaternary Science Reviews 27–28, 2530–2545.
Kennett, D.J., Kennett, J.P., West, A., Mercer, C., Que Hee, S.S., Bement, L., Bunch, T.E., Sellers, M., Wolbach, W.S., 2009. Nanodiamonds in the Younger Dryas boundary sediment. Science 323 (5910), 94.
Kim, K., 2010. Personal communication to WCM.
Komarek, E.V., Komarek, B.B., Carlyse, T.C., 1973. The Ecology of Smoke Particulates and Charcoal Residues from Forest and Grassland Fires: A Preliminary Atlas. Misc Pub 3 Tall Timbers Research Station, Tallahassee, FL.
Kucha, H., Schroll, E., Stumpfl, E.F., 2005. Fossil sulphate-reducing bacteria in the Bleiberg lead–zinc deposit, Austria. Mineralium Deposita 40, 123–126.
Kuhlbusch, T.A.J., 1995. Method for determining black carbon in residues of vegetation fires. Environmental Science & Technology 29, 2675–2695.
Lanning, F.C., Ponnaiya, B.W.X., Crumpton, C.F., 1958. The chemical nature of silica in plants. Plant Physiology 33 (5), 339–343.
Liu, Z., Otto-Bliesner, B.L., He, F., Brady, E.C., Tomas, R., Clark, P.U., Carlson, A.E., Lynch-Stieglitz, J., Curry, W., Brook, E., Erickson, D., Jacob, R., Kutzbach, J., Cheng, J., 2009. Transient simulation of last deglaciation with a new mechanism for Bølling–Allerød warming. Science 325, 310–314.
Lowe, J.J., Rasmussen, S.O., Björck, S., Hoek, W.Z., Steffensen, J.P., Walker, M.J.C., Yu, Z.C., 2008. Synchronisation of palaeoenvironmental events in the North Atlantic region during the Last Termination: a revised protocol recommended by the INTIMATE group. Quaternary Science Reviews 27, 6–17.
Mahaney, W.C., 1990. Ice on the Equator. Wm Caxton Ltd., Ellison Bay, WI. 386 pp.
Mahaney, W.C., 2002. Atlas of Sand Grain Surface Textures and Applications. Oxford University Press, Oxford, U.K. 237 pp.
Mahaney, W.C., Kalm, V., 1996. Field Guide for the International Conference on Quaternary Glaciation and Paleoclimate in the Andes Mountains. Quaternary Surveys, Toronto. 79 pp.
Mahaney, W.C., Dirszowsky, R.W., Milner, M.W., Harmsen, R., Finkelstein, S., Kalm, V., Bezada, M., Hancock, R.G.V., 2007a. Soil stratigraphy and ecological relationships of a Late Glacial–Holocene fluvial terrace sequence, Sierra Nevada National Park, Northern Venezuelan Andes. Journal of South American Earth Sciences 23, 46–60.
Mahaney, W.C., Milner, M.W., Sodhi, R.N.S., Dorn, R.I., Boccia, S., Beukens, R.P., Tricart, P., Schwartz, S., Chamorro-Perez, E., Barendregt, R.W., Kalm, V., Dirszowsky, R.W., 2007b. Analysis of burnt schist outcrops in the Alps: relation to historical archaeology and Hannibal's Crossing in 218 BC. Geoarchaeology 22, 797–816.
Mahaney, W.C., Milner, M.W., Kalm, V., Dirszowsky, R., Hancock, R.G.V., Beukens, R.P., 2008. Evidence for a Younger Dryas glacial advance in the Andes of northwestern Venezuela. Geomorphology 96, 199–211.
Mahaney, W.C., Kalm, V., Kapran, B., Milner, M.W., Hancock, R.G.V., 2009. Soil chronosequence, Humboldt Glacier, northwestern Venezuelan Andes. Geomorphology 10, 99–110.
Mahaney, W.C., Kapran, B., Milner, M.W., Kalm, V., Krinsley, D., Beukens, S., Boccia, S., Hancock, R.G.V., 2010a. Evidence from the northwestern Venezuelan Andes for extraterrestrial impact: the Black Mat enigma. Geomorphology 116 (1–2), 48–57.
Mahaney, W.C., Krinsley, D.H., Kalm, Volli, 2010b. Evidence for a cosmogenic origin of fired glaciofluvial beds in the northwestern Andes: correlation with experimentally heated quartz and feldspar. Sedimentary Geology 231, 31–40.
Maki, D., 2005. Lightning strikes and prehistoric ovens: determining the source of magnetic anomalies using techniques of environmental magnetism. Geoarchaeology 20, 449–459.
Maniloff, J., Nealson, K.H., Psenner, R., Loferer, M., Folk, R.L., 1997. Nannobacteria: size limits and evidence. Science 276 (5320), 1776–1777.
McLintock, W.F.P., 1932. On the metamorphis produced by combustion of hydrocarbons in the Tertiary sediments of south-west Russia. Mineral Magazine 23, 207–227.
Mendez, P.F., Jenkins, N.T., Eagar, T.W., 2000. Effect of electrode droplet size on evaporation and fume generation. Proc Gas Metal Arc Welding.
Nakamura, K., Fujitsuka, M., Kitajima, M., 1995. Disorder-induced line broadening in 1st-order Raman-scattering from graphite. Physical Review B 41, 12260–12263.
Napier, W.M., 2010. Palaeolithic extinctions and the Taurid Complex. Mon. Not. Royal Astronomical Society February.
National Soil Survey Center (NSSC), 1995. Soil Survey Laboratory Information Manual. Soil Survey Investigations Report No. 45. Version 1.00. USDA, Washington, DC. 305 pp.
Nealson, K.H., 1983. The microbial manganese cycle. In: Krumbein, W.E. (Ed.), Microbial Geochemistry. Blackwell, London, pp. 191–221.
Osborn, G., Clapperton, C.M., Thompson-Davis, P., Reasoner, M., Rodbell, D.T., Seltzer, G.O., Zielinski, G., 1995. Potential glacial evidence for the Younger Dryas event in the cordillera of North and South America. Quaternary Science Reviews 14, 823–832.
Oyama, M., Takehara, H., 1970. Standard Soil Color Charts. Japan Research Council for Agriculture, Forestry and Fisheries, Tokyo, Japan.
Palmgren, U., et al., 1986. Collection of airborne micro-organisms on Nuclepore filters, estimation and analysis — CAMNEA method. Journal of Applied Microbiology 61, 401–406.
Pinter, N., Ishman, S.E., 2008. Impacts, mega-tsunami, and other extraordinary claims. GSA Today 18, 37–38.
Quade, J., Forester, R.M., Pratt, W.L., Carter, C., 1998. Black Mats, spring-fed streams, and Late Glacial Age Recharge in the southern Great Basin. Quaternary Research 49, 129–148.
Ralska-Jasiewiczowa, M., Stebich, M., Negendank, J.F.W., 2001. Correlation and synchronization of Late Glacial continental sequences in northern central Europe

based on annually laminated lacustrine sediments. Quaternary Science Reviews 20, 1233–1249.
Reasoner, M.A., Osborn, G., Rutter, N.W., 1994. Age of the Crowfoot advance in the Canadian Rocky Mountains: a glacial event coeval with the Younger Dryas oscillation. Geology 22, 439–442.
Reimer, P.J., Baillie, M.G.L., Bard, E., Bayliss, A., Beck, J.W., Bertrand, C.J.H., Blackwell, P.G., Buck, C.E., Burr, G.S., Cutler, K.B., Damon, P.E., Edwards, R.L., Fairbanks, R.G., Friedrich, M., Guilderson, T.P., Hogg, A.G., Hughen, K.A., Kromer, B., McCormac, G., Manning, S., Bronk Ramsey, C., Reimer, R.W., Remmele, S., Southon, J.R., Stuiver, M., Talamo, S., Taylor, F.W., van der Plicht, J., Weyhenmeyer, C.E., 2004. IntCal04 terrestrial radiocarbon age calibration, 0–26 Cal Kyr BP. Radiocarbon 46, 1029–1058.
Rodbell, D.T., Seltzer, G.O., 2000. Rapid ice margin fluctuations during the Younger Dryas in the Tropical Andes. Quaternary Research 54, 328–338.
Salgado-Labouriau, M.L., Schubert, C., 1976. Palynology of Holocene peat bogs from the central Venezuelan Andes. Palaeogeography, Palaeoclimatology, Palaeoecology 19, 147–156.
Schopf, J.W., 1999. Cradle of Life: The Discovery of Earth's Earliest Fossils. Princeton University Press. 367 pp.
Schopf, J.W., Kudryavtsev, A.B., Agresti, D.G., Wdowiak, T.J., Czaja, A.D., 2002. Laser-Raman imagery of Earth's earliest fossils. Nature 416, 73–76.
Schubert, C., 1970. Glaciation of the Sierra de Santo Domingo, Venezuelan Andes. Quaternaria 13, 225–246.
Schubert, C., 1972. Geomorphology and glacier retreat in the Pico Bolivar area, Sierra Nevada de Mérida, Venezuela. Zeitschrift für Gletscherkunde und Glazialgeologie 8, 189–202.
Schubert, C., 1974. Late Pleistocene Mérida Glaciation, Venezuelan Andes. Boreas 3, 147–152.
Schüssler, U., Ernston, T., Ernstson, K., 2002. Impact-induced carbonate-psilomelane vein in the Azuara structure of northeastern Spain, Treb. Museum Geologica Barcelona 11, 5–65.
Shannahan, T.M., Zreda, M., 2000. Chronology of quaternary glaciations in East Africa. Earth and Planetary Science Letters 177, 23–42.
Shukla, P., Mandal, R.K., Ojha, S.N., 2001. Non-equilibrium solidification of undercooled droplets during atomization process. Bulletin of Material Science 24 (5), 547–554.
Stansell, N.D., Abbott, M.B., Polissar, J., Wolfe, A.P., Bezada, M., Rull, V., 2005. Late Quaternary deglacial history of the Mérida Andes, Venezuela. Journal of Quaternary Science 20, 801–812.
Stebbins, J.F., Du, L.-S.hu., 2002. Chloride ion sites in silicate and aluminosilicate glasses: a preliminary study by ^{35}Cl solid state NMR. American Mineralogist 87, 359–363.
Stich, A., Howard, G., Kloosterman, J.B., Firestone, R.B., West, A., Kennett, J.P., Kennett, D.J., Bunch, T.E., Wolbach, W.S., 2008. Soot as evidence for widespread fires at the Younger Dryas Onset (YDB; 12.9 ka). American Geophysical Union, fall meeting abstract no. PP13C-1471.
Teller, J.T., Leverington, D.W., Mann, J.D., 2002. Freshwater outbursts to the oceans from glacial Lake Agassiz and their role in climate change during the last deglaciation. Quaternary Science Reviews 21, 879–887.
Tilsley, J.E., 1977. Placosols: another problem in exploratory geochemistry. Journal of Geochemical Exploration 7, 21–30.
Van der Hammen, T., Hooghiemstra, H., 1995. The El Abra Stadial, a Younger Dryas equivalent in Colombia. Quaternary Science Reviews 14, 841–851.
Vortisch, W., Mahaney, W.C., Fecher, K., 1987. Lithology and weathering in a paleosol sequence on Mt. Kenya, East Africa. Geologica et Paleontologica 21, 245–255.
Westall, F., Boni, L., Guerzoni, M.E., 1995. The experimental silicification of microbes. Palaeontology 38, 495–528.
Westall, F., deWit, M.J., Dann, J., van der Gaast, S., de Ronde, C.E.J., Gerneke, D., 2001. Early Archean fossil bacteria and biofilms in hydrothermally-influenced sediments from the Barberton greenstone belt, South Africa. Precambrian Research 106, 93–116.
Wright Jr., F.W., 1999. Florida's fantastic fulgurite fire. Rocks and Minerals 74, 157–159.
Xu, H., Chen, T., Jiang, Y., Nie, Z., Liu, J., Wang, Y., 2003. Self-assembled nano-structured minerals as signatures of bacterial mineralization activities. Microscopy and Microanalysis 9, 390–391.